
Bayesian Factorised Granger-Causal Graphs For Multivariate Time-series Data

He Zhao¹ Edwin V. Bonilla¹

Abstract

We study the problem of automatically discovering Granger causal relations from observational multivariate time-series data. Vector autoregressive (VAR) models have been time-tested for this problem, including Bayesian variants and more recent developments using deep neural networks. Most existing VAR methods for Granger causality use sparsity-inducing penalties/priors or post-hoc thresholds to interpret their coefficients as Granger causal graphs. Instead, we propose a new Bayesian VAR model with a hierarchical graph prior over binary Granger causal graphs, separately from the VAR coefficients. We develop an efficient algorithm to infer the posterior over binary Granger causal graphs. Our method provides better uncertainty quantification, has less hyperparameters, and achieves better performance than competing approaches, especially on sparse multivariate time-series data.

1. Introduction

Multivariate time-series (MTS) data consist of observed samples at multiple timestamps of a set of variables/time-series and underpins a wide variety of applications in, e.g., economics, healthcare, climatology, and neuroscience. In these applications, it is important to analyse causal structures/relations between the time-series, which not only facilitates a deeper understanding of the data but also provides valuable knowledge for downstream tasks such as prediction and forecasting. In this paper, we are interested in discovering such causal relations purely from observational MTS data without conducting costly interventions.

For causal discovery on MTS data, Granger Causality (GC) (Granger, 1969; Lütkepohl, 2005; Shojaie & Fox, 2022) is a fundamental framework underlying many methods, which discovers causal relations between variables by quantifying the prediction of the future values of some variables from the past values of the others. Many GC

approaches are based on vector autoregressive (VAR) models (Lütkepohl, 2005), which assume that a time series is influenced by the (past) time lags of others and learn autoregression coefficients to capture the influences of the lags. The key to using VAR models for GC is to discover binary Granger causal relations (usually presented as sparse graphs) from their coefficients.

Recently, VAR methods based on deep learning (Montalto et al., 2015; Tank et al., 2018; Wang et al., 2018; Nauta et al., 2019; Khanna & Tan, 2020; Wu et al., 2020; Marcinkevičs & Vogt, 2021; Gong et al., 2022; Fan et al., 2023) have attracted attention by leveraging the flexibility of deep neural networks to capture more complex dynamics of MTS data. With increased model complexity, deep-learning based VAR models usually need more data to recover the true GC graphs, and may not work well under low-data regimes. Moreover, for decision making applications with discovered GC graphs, it is important to quantify the uncertainty of the links in the graph. As deep learning methods often seek for deterministic solutions, they may be less applicable to uncertainty-aware cases. Finally, causal discovery on MTS data is an unsupervised task where the ground-truth graphs are unknown and, unlike supervised learning settings, it is less clear how to construct a validation set to conduct model selection/hyperparameter tuning, typically necessary in most deep learning methods.

In the above situations, Bayesian methods gain unique advantages. Firstly, they provide a principled way of incorporating prior knowledge, which can be informative for learning from sparse MTS data. Moreover, they can naturally quantify link uncertainty via the estimated posterior distributions. Lastly, Bayesian models can be built hierarchically, reducing the need for model selection or hyperparameter tuning. This can be achieved, for example, by imposing properly-specified prior distributions on variables or using Bayesian nonparametric techniques (Orbanz & Teh, 2010; Gershman & Blei, 2012). Although Bayesian VAR models have a rich history in statistics and econometrics (Woźniak, 2016; Miranda-Agrippino & Ricco, 2019), most existing Bayesian VAR methods estimate posteriors over coefficients, which can then be transformed into binary GC graphs. However, uncertainty over these coefficients cannot be easily interpreted as uncertainty over GC graphs.

Preprint. ¹CSIRO's Data61, Australia. Correspondence to: He Zhao <he.zhao@ieee.org>.

In this paper, we propose a new Bayesian VAR method for GC that addresses the limitations of deep learning approaches and traditional VAR methods mentioned above. Specifically, we propose to model binary GC graphs directly with a Bayesian model that is separate to that of the coefficients’. In doing so, our method enjoys several benefits: **1)** We can quantify uncertainty by modelling the posterior over the GC graphs, offering a principled way to determining how likely a variable Granger-causes another. This may not be achieved by methods that use sparsity penalties (Nicholson et al., 2017; Ahelegbey et al., 2016; Ghosh et al., 2018; Billio et al., 2019) on the coefficients or use post-hoc thresholds to binarise them (Nauta et al., 2019; Marcinkevičs & Vogt, 2021). **2)** We introduce a factorised Bayesian prior with a sparsity-controlling mechanism over binary GC graphs, which samples graphs efficiently for sparse MTS data. **3)** By leveraging Bayesian nonparametric techniques and hierarchical Bayesian models, our method has fewer hyperparameters and facilitates model selection, thus being more applicable to GC discovery problems where ground-truth graphs are nonexistent.

We conduct extensive experiments over a set of benchmark datasets and compare with various VAR methods for GC. These experiments show that our approach achieves better or comparable performance than others, especially on sparse MTS datasets.

2. Background and Related Work

In this section, we recap the background on Granger causality with a focus on Vector AutoRegressive (VAR) models. For more details, we refer the readers to comprehensive surveys such as Shojaie & Fox (2022); Assaad et al. (2022); Gong et al. (2023). Consider a collection of MTS data of N time series or variables in T timestamps, stored in the matrix of $\mathbf{X} \in \mathbb{R}^{N \times T} = (\mathbf{x}_1, \dots, \mathbf{x}_T)$ where $\mathbf{x}_t \in \mathbb{R}^N$ consists of the samples/values of the N variables at timestamp $t \in \{1, \dots, T\}$. A VAR model for Granger causality (Lütkepohl, 2005; Hyvärinen et al., 2010) assumes that \mathbf{x}_t can be predicted from the τ_{\max} time lags $\{\mathbf{x}_{t-1}, \dots, \mathbf{x}_{t-\tau_{\max}}\}$ by learning a coefficient matrix $\mathbf{A}^\tau \in \mathbb{R}^{N \times N}$ for each lag $\tau \in \{1, \dots, \tau_{\max}\}$:

$$\mathbf{x}_t = \sum_{\tau=1}^{\tau_{\max}} \mathbf{A}^\tau \mathbf{x}_{t-\tau} + \epsilon_t, \quad (1)$$

where ϵ_t is an independent noise variable. Conventionally, variable j (the parent) does not Granger-cause variable i (the child) ($i, j \in \{1, \dots, N\}$) if and only if for all τ , $A_{ij}^\tau = 0$. For deterministic VARs, learning can be done by minimising a regression error: $\min_{\{\mathbf{A}^\tau\}_{\tau=1}^{\tau_{\max}}} \|\mathbf{x}_t - \sum_{\tau=1}^{\tau_{\max}} \mathbf{A}^\tau \mathbf{x}_{t-\tau}\|_2^2 + \lambda \text{reg}(\{\mathbf{A}^\tau\}_{\tau=1}^{\tau_{\max}})$ where $\text{reg}(\{\mathbf{A}^\tau\}_{\tau=1}^{\tau_{\max}})$ is a sparsity-inducing penalty e.g., a group lasso penalty (Yuan & Lin, 2006; Lozano et al., 2009):

$\sum_{i=1, j=1}^N \|A_{i,j}^\tau\|_2$. Other alternative penalties can be found at Nicholson et al. (2017).

Bayesian VARs (BVARs) are another important line of research (Breitung & Swanson, 2002; George et al., 2008; Fox et al., 2011; Ahelegbey et al., 2016; Ghosh et al., 2018; Billio et al., 2019; Nakajima & West, 2013), especially in econometrics. For more comprehensive reviews, we refer readers to Woźniak (2016); Miranda-Agrippino & Ricco (2019). A standard method may model \mathbf{x}_t with multivariate normal distributions:

$$\mathbf{x}_t \sim \mathcal{MN} \left(\sum_{\tau=1}^{\tau_{\max}} \mathbf{A}^\tau \mathbf{x}_{t-\tau}, \Sigma \right), \quad (2)$$

where various priors can be imposed on $\{\mathbf{A}^\tau\}_{\tau=1}^{\tau_{\max}}$ (e.g., sparsity-inducing priors) and Σ (e.g., Inverse-Wishart priors). Learning BVARs involves inferring the posterior of $\{\mathbf{A}^\tau\}_{\tau=1}^{\tau_{\max}}$ and Σ . Similar to deterministic VARs, one may need to “convert” $\{\mathbf{A}^\tau\}_{\tau=1}^{\tau_{\max}}$ into GC graphs.

Deep VARs have recently become popular, as they use deep neural networks to model nonlinear dynamics between timestamps (Montalto et al., 2015; Tank et al., 2018; Wang et al., 2018; Nauta et al., 2019; Khanna & Tan, 2020; Wu et al., 2020; Marcinkevičs & Vogt, 2021; Gong et al., 2022; Fan et al., 2023). They essentially generalize Eq. (1) using: $x_{it} = f_i(\sum_{\tau=1}^{\tau_{\max}} \mathbf{A}^\tau \mathbf{x}_{t-\tau}) + \epsilon_t$, where f_i is a nonlinear function typically implemented by neural networks. Different neural network architectures have been explored such as in Tank et al. (2018); Nauta et al. (2019); Khanna & Tan (2020); Marcinkevičs & Vogt (2021); Bussmann et al. (2021); Fan et al. (2023). Despite their promising performance, deep VARs may need a large number of timestamps to discover good causal graphs, require heavy model selection/parameter tuning due to the large number of parameters, and be less uncertainty-aware. More recently, Bayesian deep VARs have been proposed, such as ACD (Löwe et al., 2022), RHINO (Gong et al., 2022), and Dyn-GFN (Tong et al., 2022). Although these methods can also be considered as Bayesian approaches, their methodology and focus are quite different from ours. For example, ACD (Löwe et al., 2022) focuses on discovering causal relations across samples with different underlying causal graphs but shared dynamics. RHINO (Gong et al., 2022) extends the VAR framework by modelling instantaneous causal relations (Runge, 2020; Pamfil et al., 2020) and introducing history-dependent noise, which we do not consider in this paper. Dyn-GFN (Tong et al., 2022) is a Bayesian approach based on GFlowNets (Bengio et al., 2023) that focuses on discovering causal graphs varying with time.

In addition to VARs and Granger causality, there are other methods for discovering causal structures from MTS data but they are less closely related to ours. To capture instantaneous causal effects that are not modelled by VARs and GC,

there are functional casual models such as in Hyvärinen et al. (2010); Peters et al. (2013); Pamfil et al. (2020) and methods based on dynamic Bayesian networks (DBNs) (Dean & Kanazawa, 1989; Murphy, 2002) or structured VAR models in econometrics (Swanson & Granger, 1997; Demiralp & Hoover, 2003). For DBNs, we refer readers to surveys such as Mihajlovic & Petkovic (2001); Shiguihara et al. (2021). Moreover, there are also constraint-based approaches that extend the PC algorithm (Spirtes et al., 2000) to model time-series data (Runge, 2018; Runge et al., 2019; Runge, 2020; Huang et al., 2020).

3. Method

The key idea of our methods is to introduce a binary GC graph separately from the coefficients for each lag to a Bayesian VAR of Eq. (2), specifically:

$$\mathbf{x}_t \sim \mathcal{MN} \left(\sum_{\tau=1}^{\tau_{\max}} (\mathbf{A}^\tau \odot \mathbf{G}^\tau) \mathbf{x}_{t-\tau}, \Sigma \right), \quad (3)$$

where $\mathbf{G}^\tau \in \{0, 1\}^{N \times N}$ is the adjacency matrix for the binary GC graph of lag τ and \odot denotes the Hadamard product.

In the above model, we decouple the impact of variable j on i into two components: $A_{i,j}^\tau \in \mathbb{R}$ and $G_{i,j}^\tau \in \{0, 1\}$. If $G_{i,j}^\tau = 0$, j does not impact i in lag τ regardless of the value of $A_{i,j}^\tau$, while if $G_{i,j}^\tau = 1$, $A_{i,j}^\tau$ captures the influence from j to i . We also note that variable j does not Granger-cause variable i ($i, j \in \{1, \dots, N\}$) if and only if for all τ , $G_{i,j}^\tau = 0$. The proposed decoupling leads to several appealing benefits. First of all, we can impose an independent Bayesian prior on the GC graphs $p(\{\mathbf{G}^\tau\}_{\tau=1}^{\tau_{\max}})$ and estimate the posterior over them $p(\{\mathbf{G}^\tau\}_{\tau=1}^{\tau_{\max}} | \mathbf{X})$. This posterior offers a principled way to determine how likely a variable Granger-causes another and one can sample unlimited GC graphs from the posterior. This cannot be done by conventional VARs that induce sparsity (Nicholson et al., 2017; Ahelegbey et al., 2016; Ghosh et al., 2018; Billio et al., 2019) on the coefficients $\{\mathbf{A}^\tau\}_{\tau=1}^{\tau_{\max}}$ or use post-hoc thresholds to binarise them (Nauta et al., 2019; Marcinkevics & Vogt, 2021). Moreover, with a proper construction of $p(\{\mathbf{G}^\tau\}_{\tau=1}^{\tau_{\max}})$, one can incorporate informative prior knowledge for modelling sparse MTS data.

Despite the above benefits, learning binary graphs is a non-trivial problem. Given a binary GC graph with N variables, a naive approach might need to search from a space of $\mathcal{O}(2^{N^2})$ possible solutions. Therefore, it is important to use a suitable Bayesian prior $p(\{\mathbf{G}^\tau\}_{\tau=1}^{\tau_{\max}})$ that can lead to an efficient inference algorithm of $p(\{\mathbf{G}^\tau\}_{\tau=1}^{\tau_{\max}} | \mathbf{X})$. Before going into the core model of ours, we complete the model in Eq. (3) by imposing the following conjugate prior distributions (Miranda-Agrippino & Ricco, 2019):

$\psi_{i,j}^\tau \sim \text{Gamma}(1, 1)$, $A_{i,j}^\tau \sim \mathcal{N}(0, (\psi_{i,j}^\tau)^{-1})$ and Σ : $\lambda_i \sim \text{Gamma}(1, 1)$, $\Sigma = \text{diag}(\lambda_1, \dots, \lambda_N)^{-1}$ where $\text{diag}(\lambda_1, \dots, \lambda_N)$ returns a matrix with its diagonal elements as $\lambda_1, \dots, \lambda_N$.

3.1. Poisson Factorised Granger-Causal Graph Model

Now we introduce our Bayesian construction on GC graphs that can be integrated into VARs. To assist clarity, we discuss our method with only one lag, i.e., $\tau_{\max} = 1$, temporally omit the notation of lag τ , and introduce the extension to multiple lags later. The general idea is that we assume a binary GC graph $\mathbf{G} \in \{0, 1\}^{N \times N}$ is a sample of a probabilistic factorisation model with K latent factors: $\mathbf{G} \sim p(\Theta \Phi^T)$ where $\Theta \in \mathbb{R}_+^{N \times K}$ each entry of which $\theta_{i,k}$ indicates the weight of the k^{th} factor for variable i of being a child in a GC relation and $\Phi \in \mathbb{R}_+^{N \times K}$ each entry of which $\phi_{j,k}$ indicates the weight of the k^{th} factor for variable j of being a parent in a GC relation. In this way, whether j Granger-causes i depends on their interactions with all the K factors: $G_{i,j} \sim p\left(\sum_{k=1}^K \theta_{i,k} \phi_{j,k}\right)$. Conditioned on Θ and Φ , we have: $p(\mathbf{G} | \Theta, \Phi) = \prod_{i=1}^N \prod_{j=1}^N p(G_{i,j} | \Theta, \Phi)$, meaning that the links in \mathbf{G} can be generated independently.

As \mathbf{G} is discrete, it is natural to leverage the idea of Poisson factor analysis (PFA), a widely-used factorisation approach for discrete data (Canny, 2004; Zhou et al., 2012; Gopalan et al., 2014) with a rich set of statistical tools in probabilistic modelling and inference. As the original PFA models count-valued data with the Poisson distribution, it would be a model misspecification if this is used for binary data in our case. To address this issue, inspired by Zhou (2015), we introduce a new link function named Generalised Bernoulli Poisson Link (GBPL) that thresholds a random Poisson variable m at $V \in \{1, 2, \dots\}$ to obtain a binary variable b .

Definition 3.1. (Generalised Bernoulli Poisson Link)

$$m \sim \text{Poisson}(\gamma), b = \mathbf{1}(m \geq V),$$

where $\mathbf{1}(\cdot)$ is function returning one if the condition is true otherwise zero.

We have the following properties for GBPL:

Property 3.2. Given γ and V , one can marginalise m out to get:

$$b \sim \text{Bernoulli} \left(1 - \sum_{v=0}^{V-1} \frac{e^{-\gamma} \gamma^v}{v!} \right). \quad (4)$$

Remark. As $b = 0$ if and only if $m < V$, $p(b = 0) = \sum_{v=0}^{V-1} p(m = v)$, thus, $p(b = 1) = 1 - \sum_{v=0}^{V-1} p(m = v)$. Moreover, as $\mathbb{E}(b) = p(b = 1)$, larger V leads to lower expected probability of b being one, under the same γ .

Property 3.3. Given b , the conditional posterior of m is in close-form:

$$m \sim \begin{cases} \text{TPoisson}_V(\gamma), & \text{if } b > 0 \\ \text{Categorical}_V([\dots, f(v, \gamma), \dots]), & \text{otherwise} \end{cases}$$

where $\text{TPoisson}_V(\gamma)$ is the Poisson distribution with parameter γ left-truncated at V (i.e., the samples from that Poisson distribution are greater than or equal to V) and $f(v, \gamma) = \frac{e^{-\lambda} \lambda^v}{v!} / \sum_{v'=0}^{V-1} \frac{e^{-\lambda} \lambda^{v'}}{v'!}$ is the normalised Poisson probability mass function.

Remark. If $b > 0$, $m \geq V$ almost surely (a.s.) and one can sample m from the truncated Poisson distribution at V efficiently by computing the inverse Poisson cumulative distribution function (Giles, 2016). If $b = 0$, $m \in \{0, \dots, V-1\}$ is sampled from the categorical distribution with normalised Poisson probability masses. The close-form conditional posterior contributes to the development of an efficient algorithm of our model.

Property 3.4. When V is set to 1, GBPL reduces to the link function proposed in Zhou (2015).

Remark. Compared with the link function in Zhou (2015), GBPL is a more flexible method with an additional parameter V . As shown later, V controls the sparsity of generated graphs, which is essential for our problem.

With the help of GBPL, we propose to impose the following hierarchical Bayesian prior $p(\mathbf{G})$:

$$\begin{aligned} r_k &\sim \text{Gamma}(1/K, 1/c), \\ \theta_{i,k} &\sim \text{Gamma}(a_i, 1/d_k), \quad \phi_{j,k} \sim \text{Gamma}(b_j, 1/e_k), \\ M_{i,j} &\sim \text{Poisson}\left(\sum_{k=1}^K r_k \theta_{i,k} \phi_{j,k}\right), \quad G_{i,j} = \mathbf{1}(M_{i,j} \geq V), \end{aligned} \quad (5)$$

$$(6)$$

where noninformative gamma priors $\text{Gamma}(1, 1)$ are used for a_i, b_j, d_k, e_k , and c .

In the above model, a new variable r_k is introduced to capture the global popularity of the k^{th} factor (Yang & Leskovec, 2012; 2014; Zhou, 2015). Mathematically, the construction on Θ, Φ , and \mathbf{r} can be viewed as the truncated version of a gamma process (Ferguson, 1973; Wolpert et al., 2011; Zhou, 2015) on a product space $\mathbb{R}_+ \times \Omega$: $\mathfrak{G} \sim \Gamma\text{P}(\mathfrak{G}_{a,b}, 1/c)$, where Ω is a complete separable metric space, c is the concentration parameter, $\mathfrak{G}_{a,b}$ is a finite and continuous base measure over Ω . The corresponding Lévy measure is $\nu(dr d\theta d\phi) = r^{-1} e^{-cr} dr \mathfrak{G}_{a,b}(d\theta d\phi)$. In our case, a draw from the $\mathfrak{G}_{a,b}$ is a pair of $\theta_{:,k}$ and $\phi_{:,k}$ as shown in Eq. (5) where $\theta_{:,k} = [\theta_{1,k}, \dots, \theta_{N,k}]$, $\theta_{:,k} = [\theta_{1,k}, \dots, \theta_{N,k}]$ and $\phi_{:,k} = [\phi_{1,k}, \dots, \phi_{N,k}]$. A draw from the gamma process is a discrete distribution with countably infinite atoms from

the base measure: $\mathfrak{G} = \sum_{k=1}^{\infty} r_k \delta_{\theta_{:,k}, \phi_{:,k}}$ and r_k is the weight of the k^{th} atom. Although there are infinite atoms, the number of atoms with r_k greater than $\rho \in \mathbb{R}_+$ follows $\text{Poisson}(\int_{\rho}^{\infty} r^{-1} e^{-cr} dr)$ and the expectation of Poisson decreases when ρ increases. In other words, the number of atoms that have relatively large weights will be finite and small, thus, a gamma process based model has an inherent shrinkage mechanism. In our case, if we set the maximum number of latent factors K (i.e., the truncation level) large enough, the model will automatically learn the number of active factors.

Given the specification of the prior distributions, one can see that $\mathbb{E}(\sum_{k=1}^K r_k \theta_{i,k} \phi_{j,k}) = 1$ as $\mathbb{E}(\theta_{i,k}) = \mathbb{E}(\phi_{j,k}) = 1$ and $\mathbb{E}(r_k) = 1/K$. Therefore, according to Property 3.2 of GBPL, the expected sparsity of \mathbf{G} in the prior distribution is $N^2 \left(1 - \sum_{v=0}^{V-1} \frac{e^{-1}}{v!}\right)$. Note that $V \in \{1, 2, \dots\}$ is a natural number that controls the sparsity. Theoretically, V can be arbitrarily large, however, large V makes the sampling of the truncated Poisson distribution (Property 3.3) harder. We empirically find that when $V > 3$, the sampled GC graphs from the posterior nearly have zero links, thus, we set $V \in \{1, 2, 3\}$. Note that V is a parameter that only takes discrete values, while the regularisation weights in other VARs are usually continuous parameters taking infinite values.

Finally, we refer to the model in Eq. (3) and (6) as Poisson Factorised Granger-Causal Graph (PFGCG) and denote $\mathbf{G} \sim \text{PFGCG}(V)$. In the case of multiple lags, we summarise the model as:

$$\begin{aligned} \mathbf{G}^\tau &\sim \text{PFGCG}^\tau(V) \quad (7) \\ \mathbf{x}_t &\sim \mathcal{MN}\left(\sum_{\tau=1}^{\tau_{\max}} (\mathbf{A}^\tau \odot \mathbf{G}^\tau) \mathbf{x}_{t-\tau}, \Sigma\right), \quad (8) \end{aligned}$$

where we have a separate generative process for the GC graph at each lag τ .

3.2. Inference via Gibbs Sampling

Here we introduce how to learn PFGCG by Bayesian inference via Gibbs sampling. Recall that Gibbs sampling (Casella & George, 1992) is a widely-used Markov chain Monte Carlo (MCMC) method that takes the samples of a variable from its conditional posteriors conditioned other variables, thus, requiring ‘‘easy’’ sampling from the conditional posteriors. When it converges, the samples from a Gibbs sampler will be equivalent to those sampled from the true posterior. In our model, with the help of several augmentation techniques between Poisson and gamma distributions (Zhou et al., 2012; Zhou, 2015), PFGCG enjoys local conjugacy and all the variables have close-form conditional posteriors, which facilitate an efficient inference

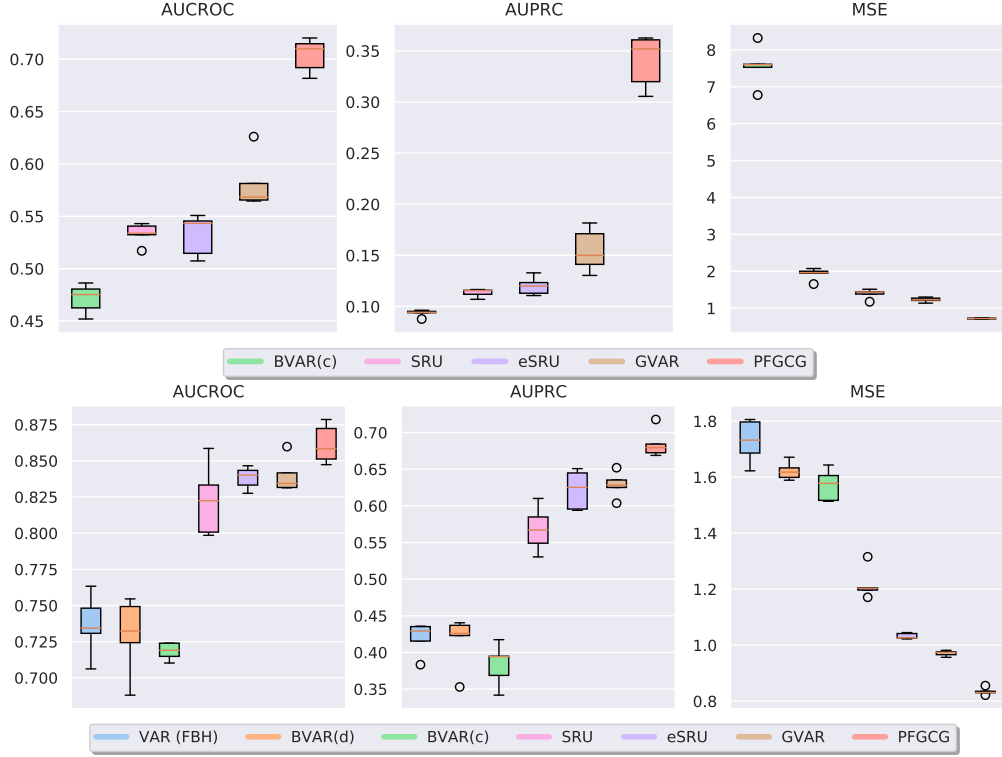


Figure 1. Results on Lorenz 96. Upper: $T = 100$, lower: $T = 500$. VAR (FBH) and BVAR(d) failed to learn when $T = 100$.

algorithm. Here we highlight the sampling of \mathbf{G}^τ and leave the other details in the appendix.

An entry $G_{i,j}^\tau$ in \mathbf{G}^τ is involved in the generative process of data as in Eq. (2) and has a Bernoulli prior according to Eq. (6). Therefore, by denoting $p(G_{i,j}^\tau = 0|-) = s_{i,j}^{\tau,0}$ and $p(G_{i,j}^\tau = 1|-) = s_{i,j}^{\tau,1}$ ($-$ stands for all the other variables), we can derive:

$$\begin{aligned}
 s_{i,j}^{\tau,0} &= \sum_{v=0}^{V-1} \frac{e^{-q_{i,j}^\tau} (q_{i,j}^\tau)^v}{v!}, \\
 s_{i,j}^{\tau,1} &= e^{-\frac{1}{2}((A_{i,j}^\tau)^2 \lambda_i U_j^\tau - 2A_{i,j}^\tau \lambda_i W_{i,j}^\tau)} (1 - s_{i,j}^{\tau,0}), \\
 G_{i,j}^\tau &\sim \text{Bernoulli} \left(\frac{s_{i,j}^{\tau,1}}{s_{i,j}^{\tau,0} + s_{i,j}^{\tau,1}} \right), \quad (9)
 \end{aligned}$$

$$\begin{aligned}
 \text{where } q_{i,j}^\tau &= \sum_{k=1}^K \theta_{i,k}^\tau r_k^\tau \phi_{j,k}^\tau, & U_j^\tau &= \sum_{t=1}^T x_{j,t-\tau}^2, \\
 W_{i,j}^\tau &= \sum_{t=1}^T x_{i,t}^{-\tau,-j} x_{j,t-\tau}, & x_{i,t}^{-\tau,-j} &= x_{i,t} - \sum_{j' \neq j}^N A_{i,j'}^\tau G_{i,j'}^\tau x_{j',t-\tau} - \sum_{\tau' \neq \tau}^{\tau_{\max}} \sum_{j'=1}^N A_{i,j'}^{\tau'} G_{i,j'}^{\tau'} x_{j',t-\tau'}.
 \end{aligned}$$

With the above conditional posterior, one can sample the entries of \mathbf{G}^τ one by one using Eq. (9). After each sample, we only need to update $W_{i,j}^\tau$ and the other statistics can be updated after all the entries are sampled. Therefore, in one

Gibbs sampling iteration, the complexity of sampling \mathbf{G}^τ is $\mathcal{O}(N^2)$.

4. Experiments

4.1. Experimental Settings

Datasets We conduct our experiments on three widely-used benchmark datasets. For each dataset we use 5 replicates and we vary $\tau_{\max} = 1, 3, 5$ for all the methods. **1) Lorenz 96** (Lorenz, 1996) is a standard benchmark synthetic MTS dataset for GC, which is generated from the following nonlinear differential equations: $\frac{dx_{i,t}}{dt} = (x_{i+1,t} - x_{i-2,t})x_{i-1,t} - x_{i,t} + F$, for $1 \leq i \leq N$, where F is a constant that models the magnitude of the external forcing. The system dynamics become increasingly chaotic for higher values of F (Karimi & Paul, 2010). Following Marcinkevičs & Vogt (2021), we set $F = 40$, which is a more difficult case. Unlike in Tank et al. (2018); Khanna & Tan (2020); Marcinkevičs & Vogt (2021), we would like to challenge the methods with sparse MTS datasets with more variables and less timestamps and set $N = 40$ and vary $T = \{200, 500\}$. **2)** Following Marcinkevičs & Vogt (2021), we evaluate the methods on another synthetic dataset generated by the Lotka–Volterra model (Bacaër & Bacaër, 2011). Again, we increase the number of variables to $N = 40$ and reduce the number of timestamps to $T = \{200, 500\}$. For

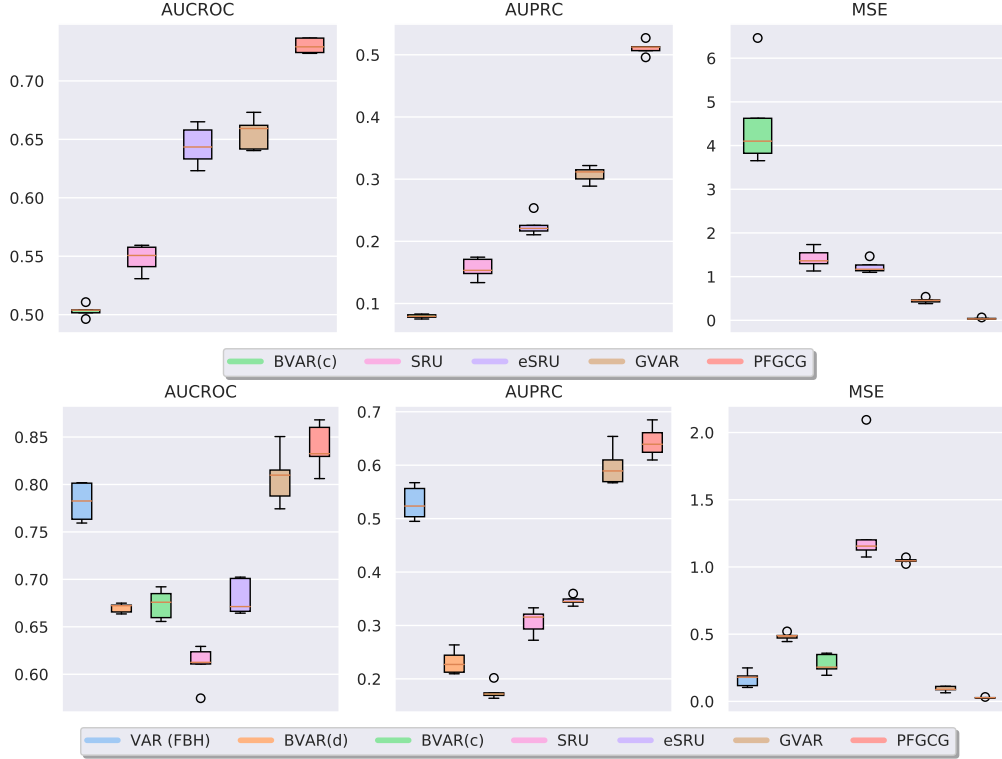


Figure 2. Results on Lotka–Volterra. Upper: $T = 200$, lower: $T = 500$. VAR (FBH) and BVAR(d) failed to learn when $T = 200$.

the other parameters of the Lotka–Volterra model, we use the same settings as in [Marcinkevičs & Vogt \(2021\)](#). **3)** We consider the fMRI dataset with realistic simulations of blood-oxygen-level dependent (BOLD) time series ([Smith et al., 2011](#)). These were generated using the dynamic causal modelling functional magnetic resonance imaging (fMRI) forward model. Following [Khanna & Tan \(2020\)](#); [Marcinkevičs & Vogt \(2021\)](#), we use 5 replicates from the simulation no. 3 of the original dataset, where $N = 15$ and $T = 200$.

Settings of Our Method To learn our model, we use 10,000 Gibbs sampling iterations where the first 5,000 are burn-in iterations and we collect the samples from the conditional posteriors after that in every 10 iterations. Specifically, we store the collections in a tensor $\mathbf{Y} \in \mathbb{R}_+^{N \times N \times \tau_{\max} \times H}$ where H is the number of collections ($H = 500$ here). For each collection $h \in \{1, \dots, H\}$, $Y[i, j, \tau, h] = \frac{s_{i,j}^{\tau,1}}{s_{i,j}^{\tau,0} + s_{i,j}^{\tau,1}}$ (Eq. (9)). The Bernoulli posterior mean of the GC graphs can be obtained by averaging $\text{mean}(\mathbf{Y}, \text{dim} = 'h')$ or one can aggregate the GC graphs of multiple lags into one by: $\text{mean}(\max(\mathbf{Y}, \text{dim} = '\tau'), \text{dim} = 'h')$ ([Marcinkevičs & Vogt, 2021](#)). As PFGCG has an intrinsic shrinkage mechanism on K , we set $K = 50$ that is empirically large enough for our experiments. The only hyperparameter of ours is V , which we vary in $\{1, 2, 3\}$.

Baselines As ours is a VAR approach for GC, we mainly include baselines that are also based on the VAR framework in our comparison. **1)** We compare with the widely-used VAR with F-tests for Granger causality and the Benjamini-Hochberg procedure ([Benjamini & Hochberg, 1995](#)) for controlling the false discovery rate (FDR) (at $q = 0.05$) denoted as VAR (FBH) and implemented in the statsmodels library ([Seabold & Statsmodels, 2010](#)). **2)** For Bayesian methods, we compare with two classic approaches based on Eq. (2) but with different prior distributions: BVAR with diffuse/noninformative priors on the coefficients (named BVAR(d)), i.e., $(\{\mathbf{A}^\tau\}_\tau^{\tau_{\max}}, \Sigma) \propto |\Sigma|^{-\frac{N+1}{2}}$ in Eq. (2) ([Litterman, 1986](#); [Miranda-Agrippino & Ricco, 2019](#)), whose posterior has an analytical form. BVAR with conjugate priors on the coefficients (named BVAR(c)): $\psi_{i,j}^\tau \sim \text{Gamma}(1, 1)$, $A_{i,j}^\tau \sim \mathcal{N}(0, (\psi_{i,j}^\tau)^{-1})$ and for Σ : $\lambda_i \sim \text{Gamma}(1, 1)$, $\Sigma = \text{diag}(\lambda_1, \dots, \lambda_N)^{-1}$. This is equivalent to an ablation of our model without $\{\mathbf{G}^\tau\}_\tau^{\tau_{\max}}$, for which we use Gibbs sampling with the same settings as ours. For deep VARs, we compare with a method with component-wise statistical recurrent units (SRU) ([Oliva et al., 2017](#)) and its improved version (economy SRU, eSRU) ([Khanna & Tan, 2020](#)) with sample-efficient architectures. The important hyperparameters of SRU and eSRU are the strengths (μ_1, μ_2, μ_3) of three regularisation terms. We also compare with GVAR ([Marcinkevičs & Vogt, 2021](#)) that uses

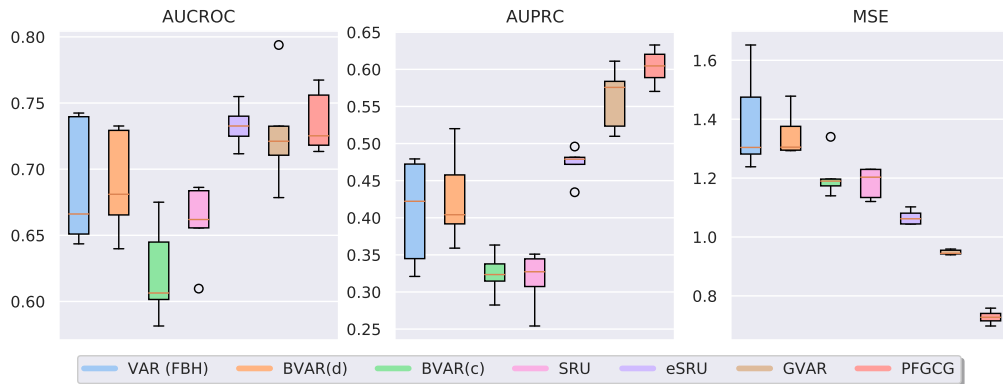


Figure 3. Results on FMRI.

Table 1. SHD for VAR (FBH), GVAR, and PFGCG. Means and standard deviations are computed over 5 replicates on each dataset.

	L96		LV		FMRI
	$T = 100$	$T = 500$	$T = 200$	$T = 500$	
VAR (FBH)	-	98.40 ± 2.42	-	74.20 ± 10.46	28.80 ± 1.33
GVAR	389.60 ± 220.64	127.40 ± 76.84	279.00 ± 104.13	82.80 ± 24.10	71.60 ± 21.82
PFGCG	117.76 ± 3.34	71.83 ± 4.07	67.01 ± 2.46	45.05 ± 4.40	24.26 ± 0.76

self-explaining neural networks (Alvarez Melis & Jaakkola, 2018) and converts the weights in the neural networks into binary GC graphs with a heuristic stability-based procedure. GVAR has achieved state-of-the-art performance. GVAR has two important regularisation hyperparameters λ and γ . For SRU, eSUR, and GVAR, the original implementations are used. For the baselines, we either use their original settings or follow these in (Marcinkevičs & Vogt, 2021), shown in Table 2 of the appendix.

Evaluation Metrics We use three metrics to compare the discovered GC graph of a method on a dataset with the ground-truth graph. For all the baseline methods, we compute the score of a discovered GC graph from their learned VAR coefficients. For our method, the score of a GC graph is the mean of the Bernoulli posterior. We report the areas under receiver operating characteristic (AUROC) and precision-recall (AUPRC) curves by comparing the score of a discovered GC graph to the ground-truth graph. Moreover, as mentioned before, VAR (FBH) and GVAR use specific post-hoc processes to convert coefficients to binary GC graphs, thus, we also report the structural Hamming distance (SHD) between the discovered binary GC graph and the ground-truth one. To compute SHD for ours, we sample a graph from the Bernoulli posterior mean. Note that unlike AUROC and AUPRC, SHD is biased to the sparsity of the ground-truth graph, e.g., for a sparse ground-truth graph, a method always predicting no links achieves low

SHD. For AUROC and AUPRC, higher values indicate better performance and for SHD, lower values are better.

Model Selection and Parameter Tuning To conduct model selection for each method, we split the input MTS data into a training set (first 80% timestamps) and a test set (remaining 20%) (Gong et al., 2022). We train a method on the training set and use the learned model to conduct one-step prediction on the test set. We then use the mean square error (MSE) on the test set and select the parameters of a method that give the best MSE. Our model selection is different from that of GVAR (Marcinkevičs & Vogt, 2021), where the best model is selected by comparing with the ground-truth graphs and report the best achievable performance. We report best MSE in our experiments as a reference but do not view it as the main metrics as our primary goal is not on predictions. The parameter space where we search for each method is shown in Table 2 of the appendix.

4.2. Results

We show the results of AUROC and AUPRC on Lorenz 96, Lotka–Volterra, and FMRI in Figure 1, 2, 3, respectively¹. The results of SHD are shown in Table 1. In general, we can see that our PFGCG performs the best on all the datasets in terms of the three metrics. Our method’s performance advan-

¹We report $\tau_{\max} = 5$ here and the results of $\tau_{\max} = 1, 3$ are in the appendix.

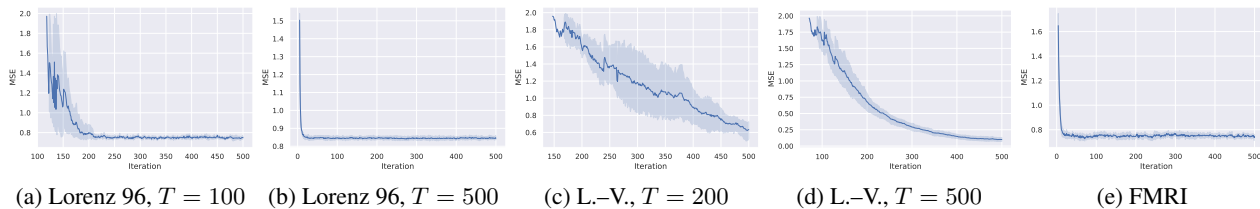


Figure 4. MSE over iterations of PFGCG ($V = 2$). For better visualisation, we only show the MSE scores in the iterations between $[a, b]$ where a is the first iteration that MSE goes below 2.0 and $b = 500$.

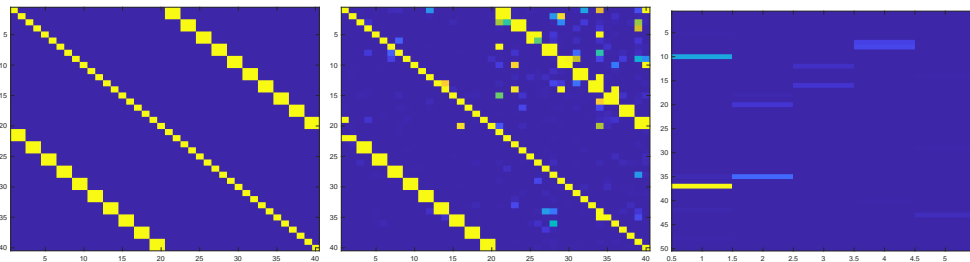


Figure 5. Qualitative analysis of PFGCG ($V = 1$, $\tau_{\max} = 5$) on Lotka–Volterra. Left: Ground-truth GC graph, middle: Bernoulli posterior mean of the discovered GC graphs, right: Matrix of $\{r_k^\tau\}_{k=1,\tau}^{K,\tau_{\max}}$. Each rectangle in the figures indicates a value of a matrix and brighter colors indicates larger values.

tage is more significant when there are less timestamps (e.g., $T = 100$ on Lorenz 96 and $T = 200$ on Lotka–Volterra), demonstrating the appealing properties of using the proposed Bayesian model on sparse MTS data. Although the mean square error (MSE) is not the focus here, our method general achieves the lowest achievable MSE as well². In the comparison between PFGCG and BVAR(c) that is equivalent to PFGCG without the binary GC graphs, one can observe that PFGCG consistently outperforms BVAR(c), showing the effectiveness of introducing binary GC graphs into the model.

Figure 4 shows the MSE of PFGCG over the inference iterations. Although we set the maximum number of Gibbs sampling iterations to 10,000, in most cases our method converges around 200 iterations. Moreover, one Gibbs iteration of PFGCG on Lorenz 96 ($T = 500$) takes less than one second running on a laptop. As Lotka–Volterra has more complex dynamics, the model may need more iterations to converge (around 2,500 iterations). We can also see that on sparser MTS data (e.g., $T = 100$ on Lorenz 96 and $T = 200$ on Lotka–Volterra), the samples of the model may have more variances in the beginning of the inference, which is as respected as there are less timestamps.

In Figure 5, we compare the Bernoulli posterior mean of PFGCG with the ground-truth graph on Lotka–Volterra. We can see that the posterior mean discovered by our method

²We do model selection for all the methods according to their MSE on the test set. Therefore, MSE reported here is just a reference.

is well aligned with the ground-truth graph, where brighter rectangles indicate higher probability of a GC link between two variables. Finally, recall that r_k^τ in Eq. (5) models the weight of latent factor k at lag τ . We plot $\{r_k^\tau\}_{k=1,\tau}^{K,\tau_{\max}}$ as a $K \times \tau_{\max}$ matrix. It can be seen that the matrix is quite sparse, where only a few entries have large values, i.e., only a few factors are active among $K = 50$. This demonstrates the shrinkage mechanism of PFGCG on K .

5. Conclusion

In this paper, we have presented a new Bayesian VAR model for Granger causal discovery on multivariate time-series data, which imposes a Poisson factorised prior (PFGCG) modelling binary GC graphs separately from the VAR coefficients. PFGCG consists of a Poisson factorisation construction that generates count-valued matrices, which are then used to generate binary GC graphs with the proposed link function (GBPL). Our model enjoys local conjugacy and Bayesian nonparametric properties, facilitating an efficient Bayesian inference algorithm with less hyperparameters. We have conducted extensive experiments comparing our method with Bayesian VARs and deep VARs, showing that ours has a significant performance advantage on sparse MTS data. Although the factorisation of PFGCG is nonlinear and our method has the potential to work well on nonlinear data (the datasets used in our experiments are nonlinear), the main limitation is that it assumes linear dynamics between timestamps, which may hinder its application on more complex data.

Impact Statements

This paper proposes a method to discover causal relations from data. The proposed method follows the assumption of Granger causality and assumes causal relations take a factorisation form. These assumptions may not hold in other data in practice and careful checks are needed when using the results of the method for decision making.

References

- Ahelegbey, D. F., Billio, M., and Casarin, R. Sparse graphical vector autoregression: A bayesian approach. *Annals of Economics and Statistics/Annales d'Économie et de Statistique*, (123/124):333–361, 2016.
- Alvarez Melis, D. and Jaakkola, T. Towards robust interpretability with self-explaining neural networks. *Advances in neural information processing systems*, 31, 2018.
- Assaad, C. K., Devijver, E., and Gaussier, E. Survey and evaluation of causal discovery methods for time series. *Journal of Artificial Intelligence Research*, 73:767–819, 2022.
- Bacaër, N. and Bacaër, N. Lotka, volterra and the predator-prey system (1920–1926). *A short history of mathematical population dynamics*, pp. 71–76, 2011.
- Bengio, Y., Lahlou, S., Deleu, T., Hu, E. J., Tiwari, M., and Bengio, E. Gflownet foundations. *Journal of Machine Learning Research*, 24(210):1–55, 2023.
- Benjamini, Y. and Hochberg, Y. Controlling the false discovery rate: a practical and powerful approach to multiple testing. *Journal of the Royal statistical society: series B (Methodological)*, 57(1):289–300, 1995.
- Billio, M., Casarin, R., and Rossini, L. Bayesian nonparametric sparse var models. *Journal of Econometrics*, 212(1):97–115, 2019.
- Breitung, J. and Swanson, N. R. Temporal aggregation and spurious instantaneous causality in multiple time series models. *Journal of Time Series Analysis*, 23(6):651–665, 2002.
- Bussmann, B., Nys, J., and Latré, S. Neural additive vector autoregression models for causal discovery in time series. In *International Conference on Discovery Science*, pp. 446–460. Springer, 2021.
- Canny, J. Gap: a factor model for discrete data. In *Proceedings of the 27th annual international ACM SIGIR conference on Research and development in information retrieval*, pp. 122–129, 2004.
- Casella, G. and George, E. I. Explaining the gibbs sampler. *The American Statistician*, 46(3):167–174, 1992.
- Dean, T. and Kanazawa, K. A model for reasoning about persistence and causation. *Computational intelligence*, 5(2):142–150, 1989.
- Demiralp, S. and Hoover, K. D. Searching for the causal structure of a vector autoregression. *Oxford Bulletin of Economics and statistics*, 65:745–767, 2003.
- Fan, C., Wang, Y., Zhang, Y., and Ouyang, W. Interpretable multi-scale neural network for granger causality discovery. In *ICASSP 2023-2023 IEEE International Conference on Acoustics, Speech and Signal Processing (ICASSP)*, pp. 1–5. IEEE, 2023.
- Ferguson, T. S. A Bayesian analysis of some nonparametric problems. *The annals of statistics*, pp. 209–230, 1973.
- Fox, E., Sudderth, E. B., Jordan, M. I., and Willsky, A. S. Bayesian nonparametric inference of switching dynamic linear models. *IEEE Transactions on signal processing*, 59(4):1569–1585, 2011.
- George, E. I., Sun, D., and Ni, S. Bayesian stochastic search for var model restrictions. *Journal of Econometrics*, 142(1):553–580, 2008.
- Gershman, S. J. and Blei, D. M. A tutorial on bayesian nonparametric models. *Journal of Mathematical Psychology*, 56(1):1–12, 2012.
- Ghosh, S., Khare, K., and Michailidis, G. High-dimensional posterior consistency in bayesian vector autoregressive models. *Journal of the American Statistical Association*, 2018.
- Giles, M. B. Algorithm 955: approximation of the inverse poisson cumulative distribution function. *ACM transactions on mathematical software (TOMS)*, 42(1):1–22, 2016.
- Gong, C., Yao, D., Zhang, C., Li, W., Bi, J., Du, L., and Wang, J. Causal discovery from temporal data. In *Proceedings of the 29th ACM SIGKDD Conference on Knowledge Discovery and Data Mining*, pp. 5803–5804, 2023.
- Gong, W., Jennings, J., Zhang, C., and Pawlowski, N. Rhino: Deep causal temporal relationship learning with history-dependent noise. *arXiv preprint arXiv:2210.14706*, 2022.
- Gopalan, P. K., Charlin, L., and Blei, D. Content-based recommendations with poisson factorization. *Advances in neural information processing systems*, 27, 2014.
- Granger, C. W. Investigating causal relations by econometric models and cross-spectral methods. *Econometrica: journal of the Econometric Society*, pp. 424–438, 1969.

- Huang, B., Zhang, K., Zhang, J., Ramsey, J. D., Sanchez-Romero, R., Glymour, C., and Schölkopf, B. Causal discovery from heterogeneous/nonstationary data. *J. Mach. Learn. Res.*, 21(89):1–53, 2020.
- Hyvärinen, A., Zhang, K., Shimizu, S., and Hoyer, P. O. Estimation of a structural vector autoregression model using non-gaussianity. *Journal of Machine Learning Research*, 11(5), 2010.
- Karimi, A. and Paul, M. R. Extensive chaos in the lorenz-96 model. *Chaos: An interdisciplinary journal of nonlinear science*, 20(4), 2010.
- Khanna, S. and Tan, V. Y. Economy statistical recurrent units for inferring nonlinear granger causality. In *International Conference on Learning Representations*, 2020.
- Litterman, R. B. Forecasting with bayesian vector autoregressions—five years of experience. *Journal of Business & Economic Statistics*, 4(1):25–38, 1986.
- Lorenz, E. N. Predictability: A problem partly solved. In *Proc. Seminar on predictability*, volume 1. Reading, 1996.
- Löwe, S., Madras, D., Zemel, R., and Welling, M. Amortized causal discovery: Learning to infer causal graphs from time-series data. In *Conference on Causal Learning and Reasoning*, pp. 509–525. PMLR, 2022.
- Lozano, A. C., Abe, N., Liu, Y., and Rosset, S. Grouped graphical granger modeling for gene expression regulatory networks discovery. *Bioinformatics*, 25(12):i110–i118, 2009.
- Lütkepohl, H. *New introduction to multiple time series analysis*. Springer Science & Business Media, 2005.
- Marcinkevičs, R. and Vogt, J. E. Interpretable models for granger causality using self-explaining neural networks. In *International Conference on Learning Representations*, 2021.
- Mihajlovic, V. and Petkovic, M. Dynamic bayesian networks: A state of the art. *University of Twente Document Repository*, 2001.
- Miranda-Agrippino, S. and Ricco, G. Bayesian vector autoregressions: Estimation. In *Oxford Research Encyclopedia of Economics and Finance*. 2019.
- Montalto, A., Stramaglia, S., Faes, L., Tessitore, G., Prevete, R., and Marinazzo, D. Neural networks with non-uniform embedding and explicit validation phase to assess granger causality. *Neural networks*, 71:159–171, 2015.
- Murphy, K. P. *Dynamic bayesian networks: representation, inference and learning*. University of California, Berkeley, 2002.
- Nakajima, J. and West, M. Bayesian analysis of latent threshold dynamic models. *Journal of Business & Economic Statistics*, 31(2):151–164, 2013.
- Nauta, M., Bucur, D., and Seifert, C. Causal discovery with attention-based convolutional neural networks. *Machine Learning and Knowledge Extraction*, 1(1):19, 2019.
- Nicholson, W. B., Matteson, D. S., and Bien, J. Varx-l: Structured regularization for large vector autoregressions with exogenous variables. *International Journal of Forecasting*, 33(3):627–651, 2017.
- Oliva, J. B., Póczos, B., and Schneider, J. The statistical recurrent unit. In *International Conference on Machine Learning*, pp. 2671–2680. PMLR, 2017.
- Orbanz, P. and Teh, Y. W. Bayesian nonparametric models. *Encyclopedia of machine learning*, 1:81–89, 2010.
- Pamfil, R., Sriwattanaworachai, N., Desai, S., Pilgerstorfer, P., Georgatzis, K., Beaumont, P., and Aragam, B. Dynotears: Structure learning from time-series data. In *International Conference on Artificial Intelligence and Statistics*, pp. 1595–1605. PMLR, 2020.
- Peters, J., Janzing, D., and Schölkopf, B. Causal inference on time series using restricted structural equation models. *Advances in Neural Information Processing Systems*, 26, 2013.
- Runge, J. Causal network reconstruction from time series: From theoretical assumptions to practical estimation. *Chaos: An Interdisciplinary Journal of Nonlinear Science*, 28(7):075310, 2018.
- Runge, J. Discovering contemporaneous and lagged causal relations in autocorrelated nonlinear time series datasets. In *Conference on Uncertainty in Artificial Intelligence*, pp. 1388–1397. PMLR, 2020.
- Runge, J., Nowack, P., Kretschmer, M., Flaxman, S., and Sejdinovic, D. Detecting and quantifying causal associations in large nonlinear time series datasets. *Science advances*, 5(11):eaau4996, 2019.
- Seabold, S. and Statsmodels, P. Econometric and statistical modeling with python. In *Proceedings of the 9th Python in science conference*, pp. 57–61, 2010.
- Shiguihara, P., Lopes, A. D. A., and Mauricio, D. Dynamic bayesian network modeling, learning, and inference: a survey. *IEEE Access*, 9:117639–117648, 2021.

- Shojaie, A. and Fox, E. B. Granger causality: A review and recent advances. *Annual Review of Statistics and Its Application*, 9:289–319, 2022.
- Smith, S. M., Miller, K. L., Salimi-Khorshidi, G., Webster, M., Beckmann, C. F., Nichols, T. E., Ramsey, J. D., and Woolrich, M. W. Network modelling methods for fmri. *Neuroimage*, 54(2):875–891, 2011.
- Spirtes, P., Glymour, C. N., Scheines, R., and Heckerman, D. *Causation, prediction, and search*. MIT press, 2000.
- Swanson, N. R. and Granger, C. W. Impulse response functions based on a causal approach to residual orthogonalization in vector autoregressions. *Journal of the American Statistical Association*, 92(437):357–367, 1997.
- Tank, A., Covert, I., Foti, N., Shojaie, A., and Fox, E. Neural granger causality for nonlinear time series. *stat*, 1050:16, 2018.
- Tong, A., Atanackovic, L., Hartford, J., and Bengio, Y. Bayesian dynamic causal discovery. In *A causal view on dynamical systems, NeurIPS 2022 workshop*, 2022.
- Wang, Y., Lin, K., Qi, Y., Lian, Q., Feng, S., Wu, Z., and Pan, G. Estimating brain connectivity with varying-length time lags using a recurrent neural network. *IEEE Transactions on Biomedical Engineering*, 65(9):1953–1963, 2018.
- Wolpert, R. L., Clyde, M. A., Tu, C., et al. Stochastic expansions using continuous dictionaries: Lévy adaptive regression kernels. *The Annals of Statistics*, 39(4):1916–1962, 2011.
- Woźniak, T. Bayesian vector autoregressions. *Australian Economic Review*, 49(3):365–380, 2016.
- Wu, T., Breuel, T., Skuhersky, M., and Kautz, J. Discovering nonlinear relations with minimum predictive information regularization. *arXiv preprint arXiv:2001.01885*, 2020.
- Yang, J. and Leskovec, J. Community-affiliation graph model for overlapping network community detection. In *2012 IEEE 12th international conference on data mining*, pp. 1170–1175. IEEE, 2012.
- Yang, J. and Leskovec, J. Structure and overlaps of ground-truth communities in networks. *ACM Transactions on Intelligent Systems and Technology (TIST)*, 5(2):1–35, 2014.
- Yuan, M. and Lin, Y. Model selection and estimation in regression with grouped variables. *Journal of the Royal Statistical Society Series B: Statistical Methodology*, 68(1):49–67, 2006.
- Zhou, M. Infinite edge partition models for overlapping community detection and link prediction. In *AISTATS*, pp. 1135–1143, 2015.
- Zhou, M. and Carin, L. Negative binomial process count and mixture modeling. *IEEE Transactions on Pattern Analysis and Machine Intelligence*, 37(2):307–320, 2013.
- Zhou, M., Hannah, L., Dunson, D., and Carin, L. Beta-negative binomial process and poisson factor analysis. In *Artificial Intelligence and Statistics*, pp. 1462–1471. PMLR, 2012.

A. Appendix

A.1. Inference via Gibbs Sampling

Sampling A^τ With the conjugacy of normal distributions, one can sample the entries of A^τ one by one by:

$$A_{i,j}^\tau \sim \begin{cases} \mathcal{N}(0, (\psi_{i,j}^\tau)^{-1}), & \text{if } G_{i,j}^\tau = 0 \\ \mathcal{N}(\mu_{i,j}^\tau, \sigma_{i,j}^\tau), & \text{otherwise} \end{cases} \quad (10)$$

where:

$$\sigma_{i,j}^\tau = \left(\lambda_i G_{i,j}^\tau \sum_{t=1}^T x_{j,t-\tau}^2 + \psi_{i,j}^\tau \right)^{-1}, \quad (11)$$

$$\mu_{i,j}^\tau = \sigma_{i,j}^\tau G_{i,j}^\tau \lambda_i \left(\sum_{t=1}^T x_{i,t}^{\neg\tau, \neg j} x_{j,t-\tau} \right), \quad (12)$$

$$x_{i,t}^{\neg\tau, \neg j} = x_{i,t} - \sum_{j' \neq j} A_{i,j'}^\tau G_{i,j'}^\tau x_{j',t-\tau} - \sum_{\tau' \neq \tau} \sum_{j'=1}^N A_{i,j'}^{\tau'} G_{i,j'}^{\tau'} x_{j',t-\tau'} \quad (13)$$

Sampling $\psi_{i,j}^\tau$ and λ_i With the conjugacy between normal and gamma distributions, one can sample $\psi_{i,j}^\tau$ and λ_i from their conditional gamma posteriors:

$$\psi_{i,j}^\tau \sim \text{Gamma}(1.5, 1/(A_{i,j}^\tau/2 + 1)), \quad (14)$$

$$\lambda_i \sim \text{Gamma} \left(1 + T/2, \left(1 + \sum_{t=1}^T (x_{i,t} - \sum_{\tau=1}^{\tau_{\max}} \sum_{j=1}^N A_{i,j}^\tau G_{i,j}^\tau x_{j,t-\tau}) \right)^{-1} \right). \quad (15)$$

Sampling M^τ With GBPL, we can sample:

$$M_{i,j}^\tau \sim \begin{cases} \text{Categorical}_V \left(\left[\dots, \frac{e^{-q_{i,j}^\tau} (q_{i,j}^\tau)^v}{v!} \sum_{v'=0}^V \frac{e^{-q_{i,j}^\tau} (q_{i,j}^\tau)^{v'}}{v'!}, \dots \right] \right), & \text{if } G_{i,j}^\tau = 0 \\ \text{TPoisson}_V(q_{i,j}^\tau), & \text{otherwise} \end{cases} \quad (16)$$

where $q_{i,j}^\tau = \sum_{k=1}^K \theta_{i,k}^\tau r_k^\tau \phi_{j,k}^\tau$.

Sampling $M_{i,j,k}^\tau$ With the relationships between Poisson and multinomial distributions, we can sample:

$$[\dots, m_{i,j,k}^\tau, \dots] \sim \text{Multinomial}_K \left(m_{i,j}^\tau; \left[\dots, \frac{q_{i,j,k}^\tau}{\sum_{k'=1}^K q_{i,j,k'}^\tau}, \dots \right] \right), \quad (17)$$

where $q_{i,j,k}^\tau = \theta_{i,k}^\tau r_k^\tau \phi_{j,k}^\tau$.

Sampling $\theta_{i,k}^\tau$, $\phi_{j,k}^\tau$, and r_k^τ

$$\theta_{i,k}^\tau \sim \text{Gamma} \left(a_i^\tau + \sum_{j=1}^N M_{i,j,k}^\tau, \frac{1}{d_k^\tau + r_k^\tau \sum_{j=1}^N \phi_{j,k}^\tau} \right), \quad (18)$$

$$\phi_{j,k}^\tau \sim \text{Gamma} \left(b_j^\tau + \sum_{i=1}^N M_{i,j,k}^\tau, \frac{1}{e_k^\tau + r_k^\tau \sum_{i=1}^N \theta_{i,k}^\tau} \right), \quad (19)$$

$$r_k^\tau \sim \text{Gamma} \left(1/K + \sum_{i=1}^N \sum_{j=1}^N M_{i,j,k}^\tau, \frac{1}{c^\tau + \sum_{i=1}^N \sum_{j=1}^N \theta_{i,k}^\tau \phi_{j,k}^\tau} \right). \quad (20)$$

Table 2. Hyperparameter settings.

Model	τ_{\max}	# hidden layers	# hidden units	# training epochs	Learning rate	Mini-batch size	Parameter space
VAR (FBH)	{1,3,5}	NA	NA	NA	NA	NA	NA
BVAR(d)	{1,3,5}	NA	NA	NA	NA	NA	NA
BVAR(c)	{1,3,5}	NA	NA	NA	NA	NA	NA
SRU	NA	1	10	2000	1.0e-3	50	$\mu_1 = [0.01, 0.05]$ $\mu_2 = [0.01, 0.05]$ $\mu_3 = [0.01, 1.0]$
eSRU	NA	2	10	2000	1.0e-3	50	$\mu_1 = [0.01, 0.05]$ $\mu_2 = [0.01, 0.05]$ $\mu_3 = [0.01, 1.0]$
GVAR	{1,3,5}	2	50	1,000	1.0e-4	64	$\lambda = [0.0, 3.0]$ $\gamma = [0.0, 0.1]$
PFGCG	{1,3,5}	NA	NA	10,000	NA	NA	$V = \{1, 3, 5\}$

 Table 3. SHD for VAR (FBH), GVAR, and PFGCG with $\tau_{\max} = 1$. Means and standard derivations are computed over 5 replicates on each dataset.

	L96		LV		FMRI
	$T = 100$	$T = 500$	$T = 200$	$T = 500$	
VAR (FBH)	-	72.00±4.69	125.60±21.88	451.40±69.85	26.00±1.10
GVAR	373.20±39.77	93.60±55.23	147.80±80.36	111.00±39.75	51.00±16.79
PFGCG	112.91±1.95	71.43±3.52	186.13±21.84	49.73±4.72	25.17±1.43

Sampling a_i^τ and b_j^τ By introducing auxiliary variables from the Chinese Restaurant Table (CRT) distribution (Zhou et al., 2012; Zhou & Carin, 2013), we can sample:

$$l_{i,k}^\tau \sim \text{CRT} \left(\sum_{j=1}^N M_{i,j,k}^\tau, a_i^\tau \right), \quad (21)$$

$$a_i^\tau \sim \text{Gamma} \left(1 + \sum_{k=1}^K l_{i,k}^\tau, \frac{1}{1 + \sum_{k=1}^K \log(1 + r_k^\tau \sum_{j=1}^N \phi_{j,k}^\tau / d_k^\tau)} \right), \quad (22)$$

$$o_{j,k}^\tau \sim \text{CRT} \left(\sum_{i=1}^N M_{i,j,k}^\tau, b_j^\tau \right), \quad (23)$$

$$b_j^\tau \sim \text{Gamma} \left(1 + \sum_{k=1}^K o_{j,k}^\tau, \frac{1}{1 + \sum_{k=1}^K \log(1 + r_k^\tau \sum_{i=1}^N \theta_{i,k}^\tau / e_k^\tau)} \right). \quad (24)$$

Sampling d_k^τ , e_k^τ and c^τ

$$d_k^\tau \sim \text{Gamma} \left(\sum_{i=1}^N a_i^\tau + 1, \frac{1}{\sum_{i=1}^N \theta_{i,k}^\tau + 1} \right), \quad (25)$$

$$e_k^\tau \sim \text{Gamma} \left(\sum_{j=1}^N b_j^\tau + 1, \frac{1}{\sum_{i=1}^N \phi_{j,k}^\tau + 1} \right), \quad (26)$$

$$c^\tau \sim \text{Gamma} \left(2, \frac{1}{\sum_{k=1}^K r_k^\tau + 1} \right). \quad (27)$$

A.2. More Results

Algorithm 1: Inference Algorithm for PFGCG.

```

input : MTS data  $X$ , number of lags  $\tau_{\max}$ , hyperparameter  $V$ 
output : Posterior samples of  $\{A^\tau\}_\tau^{\tau_{\max}}$  and  $\{G^\tau\}_\tau^{\tau_{\max}}$ 
Initialise all the variables;
while Not converged do
    for  $i = 1 \dots N$  do
        | Sample  $\lambda_i$ ;
    end
    for  $\tau = 1 \dots \tau_{\max}$  do
        for  $i = 1 \dots N, j = 1 \dots N$  do
            | Sample  $M_{i,j}^\tau$  and  $M_{i,j,k}^\tau$ ;
        end
        Sample  $c^\tau$ ;
        for  $i = 1 \dots N$  do
            | Sample  $a_i^\tau$  and  $b_i^\tau$ ;
        end
        for  $k = 1 \dots K$  do
            | Sample  $d_k^\tau, e_k^\tau, r_k^\tau$ ;
        end
        for  $i = 1 \dots N$  do
            | for  $k = 1 \dots K$  do
                | Sample  $\theta_{i,k}^\tau$  and  $\phi_{i,k}^\tau$ ;
            end
        end
        for  $i = 1 \dots N$  do
            | for  $j = 1 \dots N$  do
                | Sample  $A_{i,j}^\tau, \psi_{i,j}^\tau, G_{i,j}^\tau$ ;
            end
        end
    end
end

```

Table 4. SHD for VAR (FBH), GVAR, and PFGCG with $\tau_{\max} = 3$. Means and standard derivations are computed over 5 replicates on each dataset.

	L96		LV		FMRI
	$T = 100$	$T = 500$	$T = 200$	$T = 500$	
VAR (FBH)	-	79.60±3.32	84.40±4.18	75.40±5.85	25.80±1.33
GVAR	577.40±47.51	133.20±107.22	213.80±117.98	128.60±68.31	50.00±18.99
PFGCG	114.75±1.68	73.18±2.67	75.30±9.21	45.50±2.34	24.78±1.08

Bayesian Factorised Granger-Causal Graphs For Multivariate Time-series Data

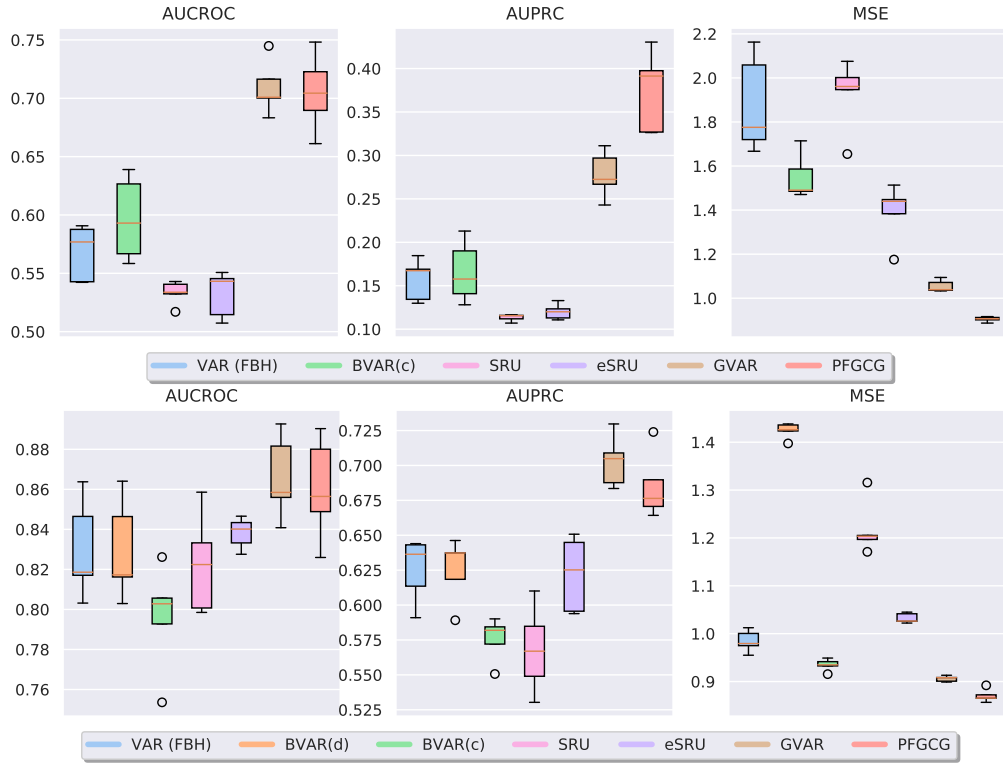


Figure 6. Lorenz 96 with $\tau_{\max} = 1$. Upper: $T = 100$, lower: $T = 500$. VAR (FBH) and BVAR(d) failed to learn when $T = 100$.



Figure 7. Lorenz 96 with $\tau_{\max} = 3$. Upper: $T = 100$, lower: $T = 500$. BVAR(d) failed to learn when $T = 100$.

Bayesian Factorised Granger-Causal Graphs For Multivariate Time-series Data

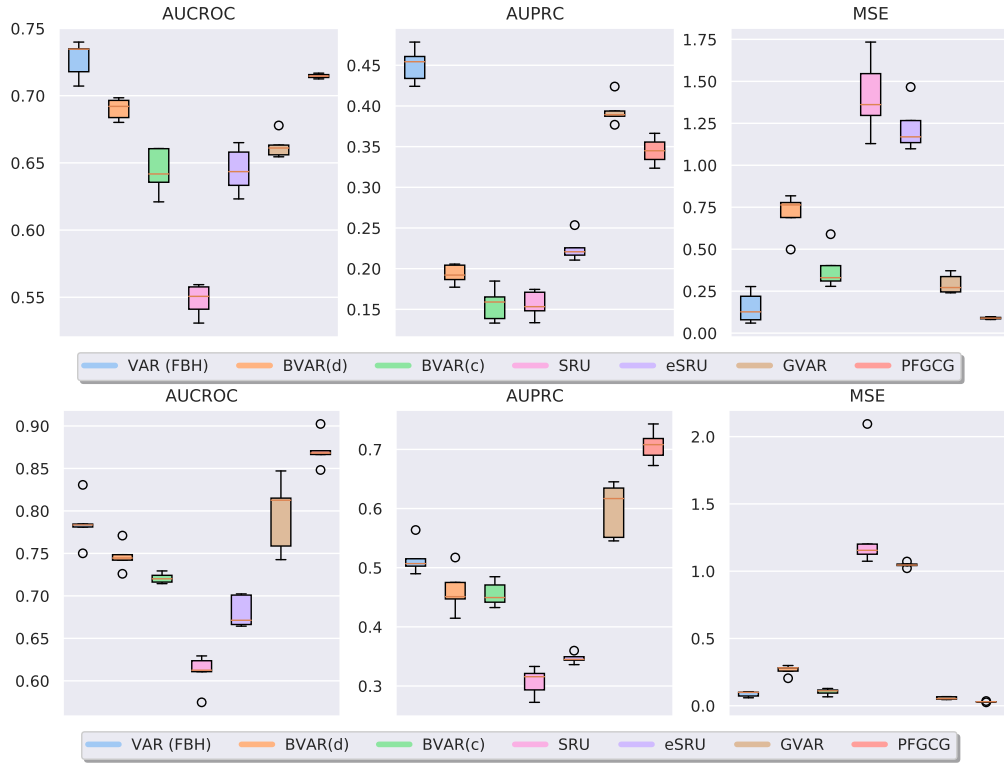


Figure 8. Lotka–Volterra with $\tau_{\max} = 1$. Upper: $T = 200$, lower: $T = 500$.

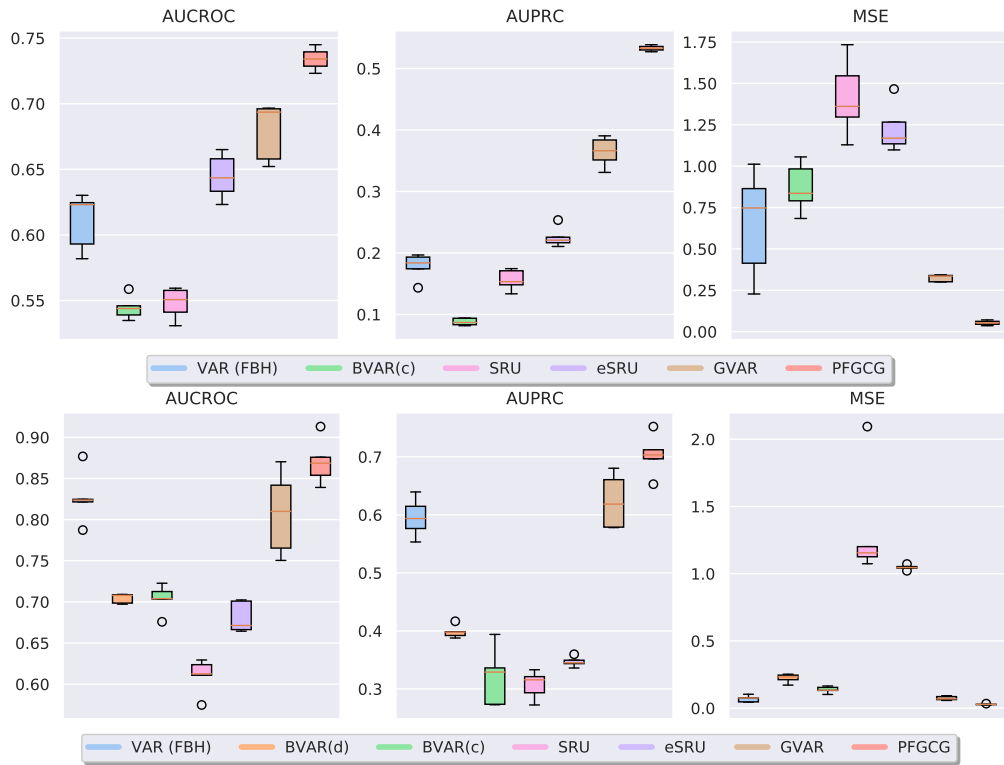


Figure 9. Lotka–Volterra with $\tau_{\max} = 3$. Upper: $T = 200$, lower: $T = 500$. VAR (FBH) and BVAR(d) failed to learn when $T = 200$.

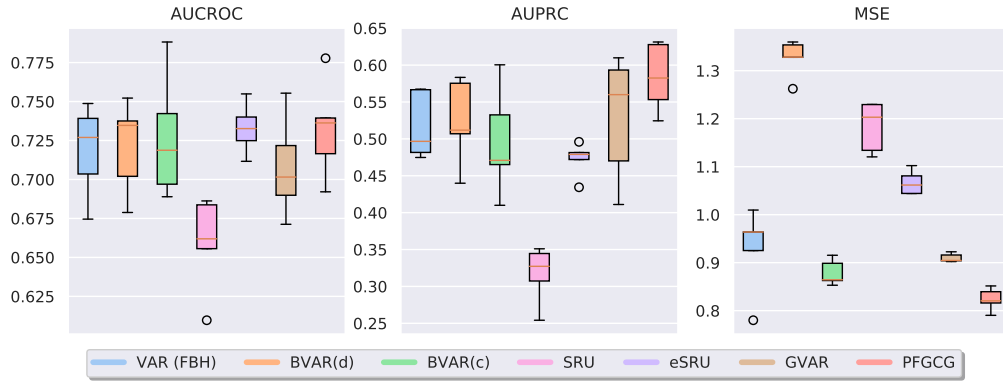


Figure 10. FMRI with $\tau_{\max} = 1$.

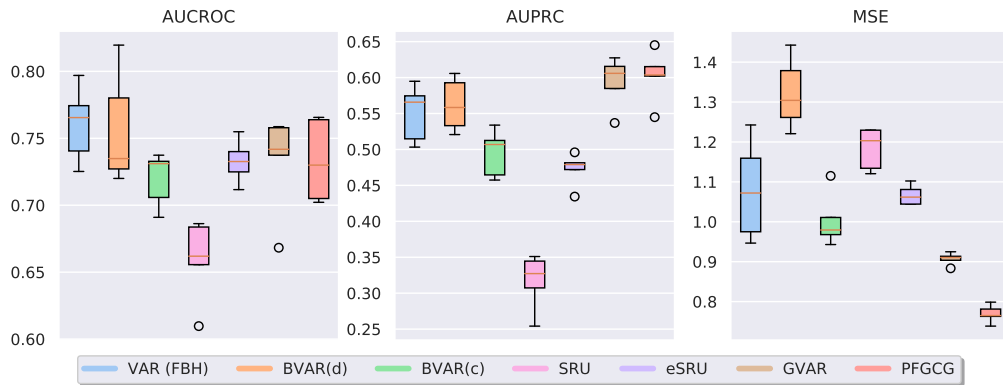


Figure 11. FMRI with $\tau_{\max} = 3$.